Feasibility Study of Multi Objective Shape Optimization for

Rocket Engine Turbopump Blade Design

Naoki Tani[1]
Japan Aerospace Exploration Agency, Tsukuba-Shi, Ibaraki, 305-8505, JAPAN

Akira Oyama[2]
Institute of Space and Astronautical Science, Japan Aerospace Exploration Agency Sagamihara, Kanagawa, 229-8510, JAPAN

Koichi Okita[3]
Japan Aerospace Exploration Agency, Tsukuba-Shi, Ibaraki, 305-8505, JAPAN

and

Nobuhiro Yamanishi[4]
Japan Aerospace Exploration Agency, Tsukuba-Shi, Ibaraki, 305-8505, JAPAN

JAXA is now planning to develop a next generation booster engine named LE-X, which is a successor of LE-7A. From an engine cycle study, the LE-X requires a relatively high efficiency turbopump. To achieve this requirement, a feasibility study of design optimization with generic algorithm was applied to the impeller and turbine blade shape. As the first step, single objective optimization was carried out on the impeller blade design, and the second one was a multi objective optimization on the turbine blade shape. It was concerned that optimization may not be effective in such a highly loaded component, however, each of the optimized result have shown improvement on performance. Especially, multi objective optimization can show tradeoff information for several important parameters, therefore, it can be said that such method is quite useful for the improvement or the developing of high efficiency turbopumps.

Nomenclature

Corr	=	Correlation function
H	=	Blade Height
M	=	Total moment
m(r)	=	Local moment at radius r
m_f	=	Mass flow rate
P_{PS}	=	Pressure surface blade surface pressure
P_{SS}	=	Suction surface blade surface pressure
R	=	Radius
R_{tip}	=	Tip Radius
U	=	Tangential velocity
ΔU	=	Tangential velocity difference between inlet and outlet

---

[1] Engineer, JAXA's Engineering Digital Innovation Center, 2-1-1 Sengen , Member AIAA
[2] Assistant professor, Department of Space Transportation Engineering, 3-1-1 Yoshinodai, Member AIAA
[3] Senior Engineer, Space Transportation Engineering Department, 2-1-1 Sengen, Member AIAA
[4] Associate Senior Engineer, JAXA's Engineering Digital Innovation Center, 2-1-1 Sengen , Member AIAA

I. Introduction

IN order to achieve high-efficiency and high-robustness, the expander-bleed cycle was chosen as an engine cycle for the next generation booster engine, called LE-X (Fig.1)[1][2]. The LE-X is considered to use liquid-hydrogen as a fuel, and liquid-oxygen as an oxidizer. The energy source of the driving gas for the turbo-pump is generated by the heat-exchange around the main combustion chamber in expander-bleed cycle, thus high efficiency pumps and turbines are required. [1]
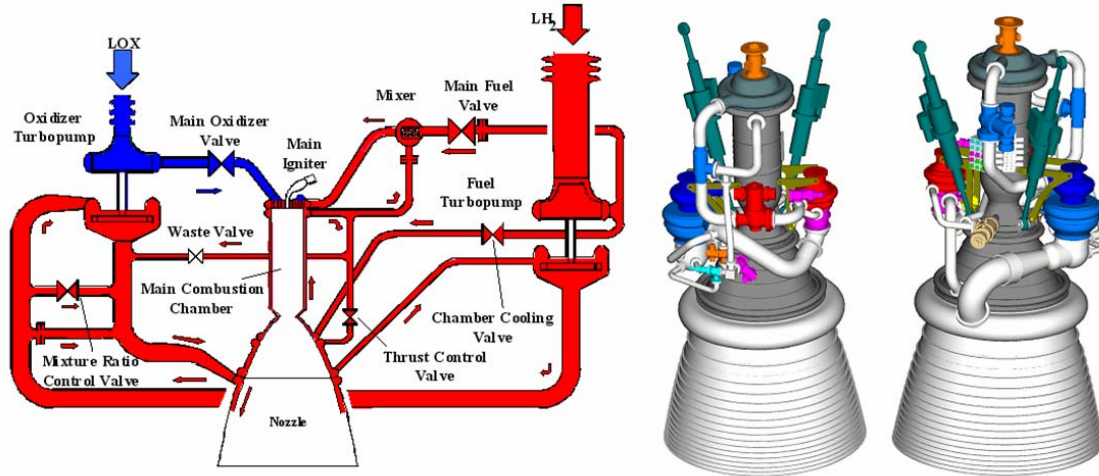

Fig. 1. LE-X Cycle Diagram and 3D Model

The shape optimization is considered to be one of the best way to achieve the above objective. Usually, engineering problems are tradeoff problems, such as weight and structural strength. Presently, multi-objective genetic algorithm (MOGA) was chosen as an optimization method since MOGA can handle multi objective optimization problem and can search through a large design space. In a gas-turbine and airplane design, effectiveness of MOGA is widely demonstrated in applications such as a compressor [3], a turbine [4] and a cooling system [5]. However, compared to the conventional turbo-machinery, the rocket turbopump must be small and have high-rotational speed. As a result, both the impeller and the turbine become highly loaded, thus, there is a question that whether the shape optimization of such a highly loaded cascade can be improved or not. Especially, the efficiency of the impeller and the turbine are interdependent, and improvement of both of them at a same time is quite important. However, such an optimization is quite heavy calculation, therefore, in the present study, shape optimization of each component was carried out on a trial base. As the first step, single objective optimization was applied to the impeller blade. After the confirmation of the single objective optimization, the MOGA was applied to the turbine blade shape optimization. In order to clarify the trade-off information in MOGA, Self Organizing Map (SOM) [6] was applied to show its effectiveness to the engineering problem. SOM can graphically show multi-dimensional trade-off information by projecting to a two-dimensional map.

II. Computational Method

The presently used optimization method is a real-coded multi-objective generic algorithm with constraint-handling method by Oyama et al.[7]. One of the features of this method is that it is more efficient and more robust on searching the optimized solution with multiple constraints. The parameters of MOGA are listed in Table 1.

As a CFD solver, the commercial code FLUENT 6.3.29 was used. Presently, both the impeller and the turbine calculations used the same computational methods.
- Pressure-Velocity Coupling Method : Compressible/Incompressible SIMPLE Algorism
- Advection Scheme : Second-order Upwind
- Turbulence Model : Realizable k-ε Model + Non-equilibrium Wall Function

The boundary conditions will be mentioned in the each chapter.

As for the shape optimization, computational mesh deformation technique is required, and the grid morphing software SCULPTOR1.8.7 was used in the present study. The grid morphing technique has several advantages as follows: one is that complicated grid re-generation method is not necessary, and this method only needs initial grid generation and definition of the control points. The other is a system generality, since shape optimization can be carried out only by defining morphing control points. The flowchart of the present optimization is shown in Fig.2.

Table 1. Generic Algorithm Methods and Parameters

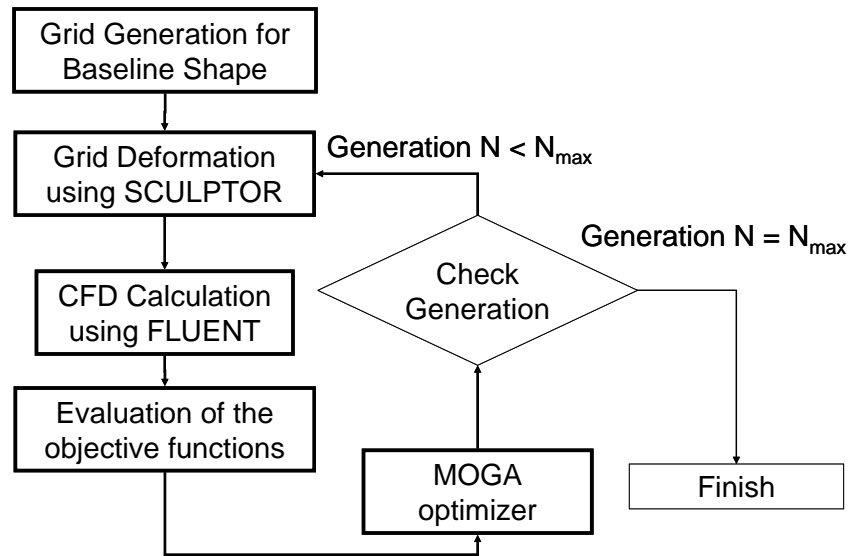| Fitness	Pareto Ranking + Shearing
Selection	SUS
Crossover	BLX-0.5
Alternation of Generation	Best-N
Mutation Rate	0.2
Population No.	16

Fig.2 Flowchart of the Present Optimization

III. Single Objective Optimization on the Impeller Blade

A. Design Problem and Computational Condition

In order to confirm the effectiveness of the optimization by the genetic algorithm, single objective optimization on the impeller was carried out as the first step. The baseline shape and computational grid of the impeller are shown in Fig.3. The present calculation is a single passage with periodic condition, and the grid number is 410,000 with about 300 wall $Y+$ value. The impeller is the first stage impeller of the LE-7A fuel turbo-pump. The specific speed of the impeller is quite small and the impeller diameter should be small for mass reduction, consequently the blade loading becomes quite high. Practically, a pump head is a requirement for the design of a pump impeller, and lower

driving horsepower is recommended. Therefore, the following objective function and constraint condition are considered.

- Objective function
  - Shaft Horsepower: Minimize
- Constraint Function
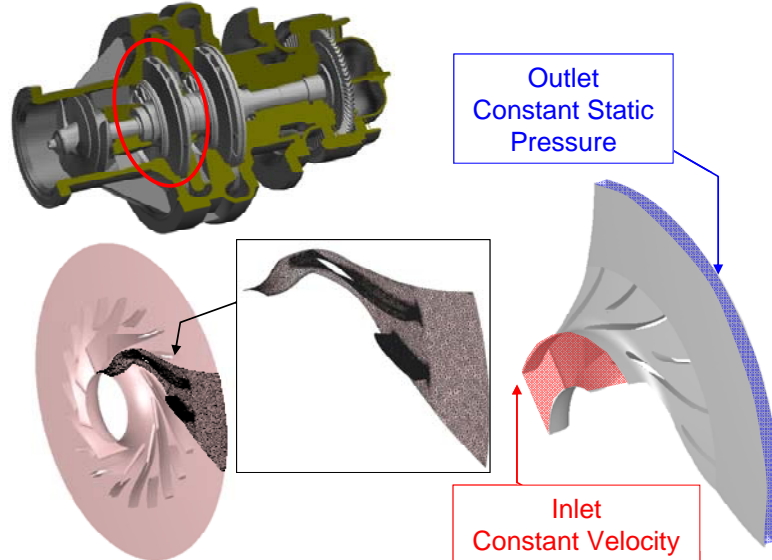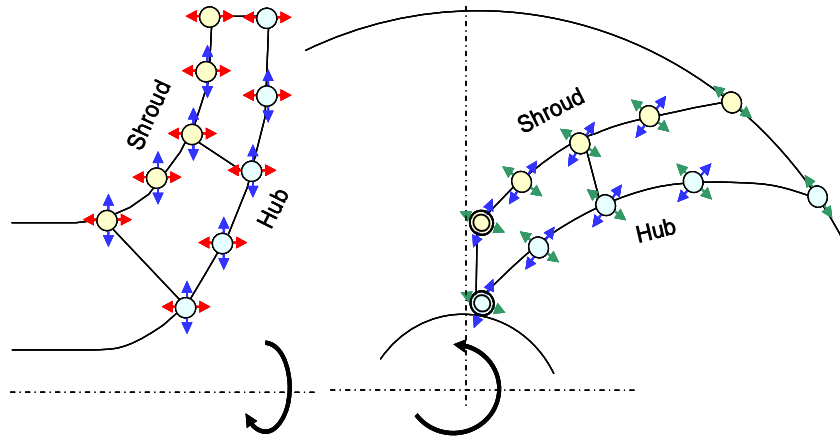 - Total Head Rise: Constant

Fig.3 Baseline Shape

Fig.4 Control Points distribution
Left: Meridional Plane. Right: Front View.

For shape deformation, control points should be defined, and the blade shape is changed by moving these control points. Figure 4 shows the distribution of the control points. There are 5 control points in hub and shroud section, and each control point moves in the axial, radial and circumferential direction. However, to maintain the impeller radius constant, the trailing edge control points do not move in the radial direction. The splitter vane is always located at the center. The total design variables are 28.

The rotation speed is set to about 42000 rpm and the working fluid is liquid hydrogen. There is an inducer and guide vane upstream of the impeller, therefore, inlet velocity distribution, which is obtained from the total stage analysis [8], is superimposed at the inlet boundary condition. The total generation is set to 50.

B. Optimized Results

Figure 5 shows the history of the objective function, and this figure shows that the shaft horsepower becomes lower as the generation number becomes larger. There are quite few feasible results in the initial generations, and

the performance of these few feasible results are worth than that of the original shape. As the generation change proceeds, the feasible results are gradually increased and the impeller performance, namely shaft horsepower, becomes better. In the final generation, the shaft horsepower becomes 4.4% lower than that of the original shape.
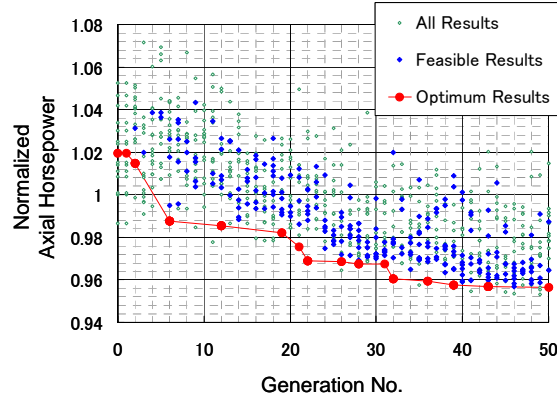

Fig.5 Optimization History.
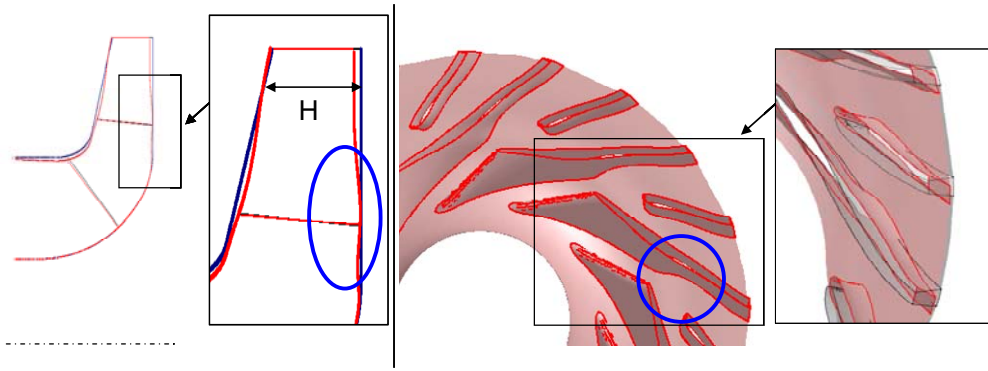The axial-horsepower is normalized by the baseline shape result.

Fig.6 Optimized Shape
Left: Meridional Plane. Right: Front View.
The black lines show the baseline shape. The blue circle shows dent position.

The blade shape of the optimum result is shown in Fig. 6. It can be clearly observed that the blade shape of the optimized result becomes the concave shape at the blade suction side. And there is also a concave at the hub surface. The shaft-horsepower is primarily a sum of the moment on blade surface, therefore, comparison of the moment at each radius should be compared. The pressure difference between the pressure and the suction surface of the blade is a primary source of the moment, and viscous force is negligibly small. Therefore, moment can be calculated as following.

$$M = \int R \cdot (P_{PS} - P_{SS}) H(R) \cdot dR = \sum m(R) \qquad (1)$$

$$m(R) = R \cdot (P_{PS} - P_{SS}) H(R) \cdot \Delta R \qquad (2)$$

The definition of H is described in Fig.6. Figure 7 shows pressure and local moment distribution on the main (long) and splitter(short) blade near the impeller exit. The pressure is normalized by baseline impeller total pressure head, and the local moment is normalized by the baseline shape total moment. The moment of the short blade is not greatly changed, but the local moment of the long blade becomes smaller in the wide area around the tip region. The pressure distribution is not greatly changed. According to Fig.6, blade height H of the optimized shape becomes smaller than that of the original one, and it can be said that this is a primary reason of the reduction of total moment, namely shaft-horsepower.
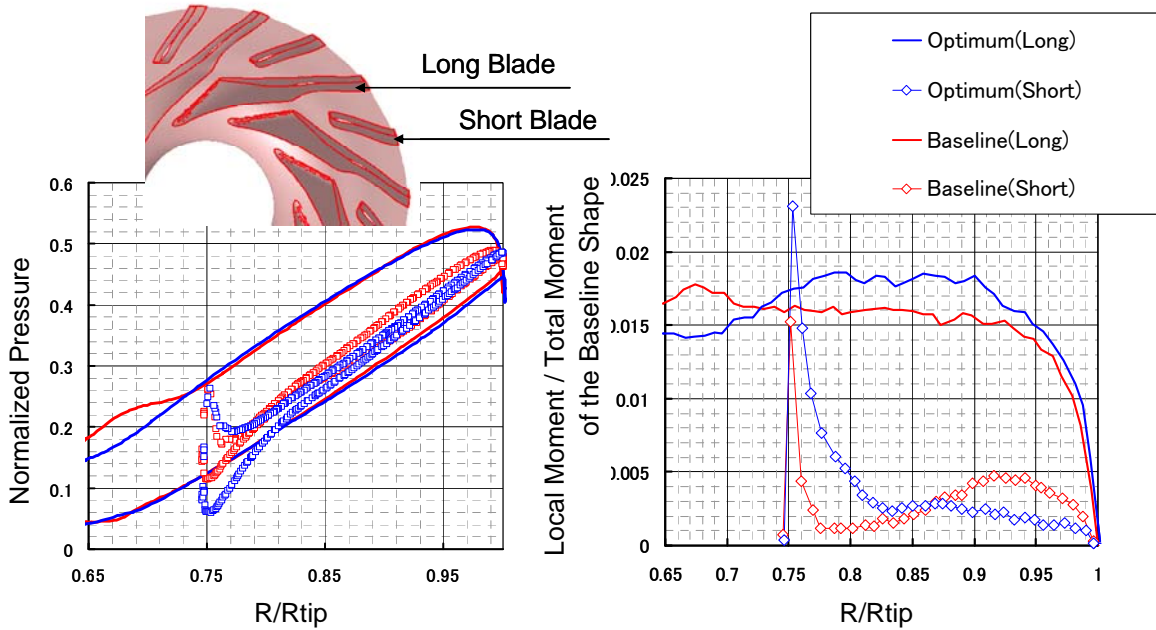
American Institute of Aeronautics and Astronautics

Fig.7 Pressure Distribution at the Mid-Span (Left) and Local Moment Distribution (Right)
Pressure is normalized by total pressure rise.

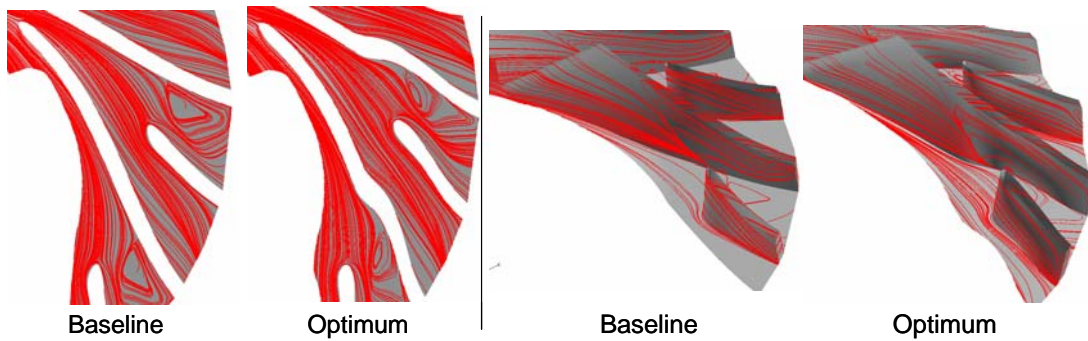Baseline   Optimum   Baseline   Optimum

Fig.8 Relative Surface Streamline Comparison
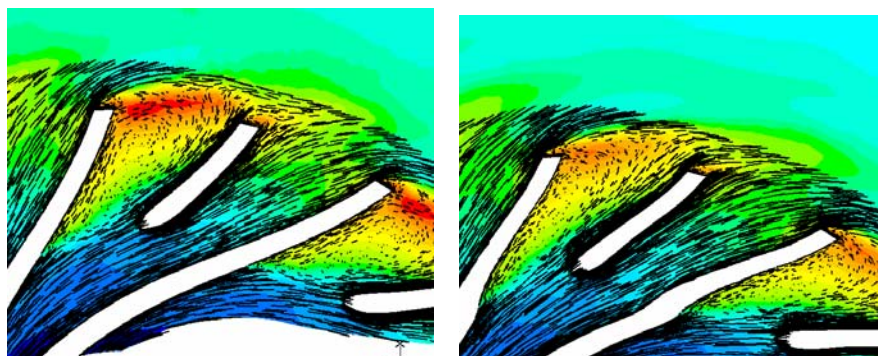Left : Hub surface   Right: Suction Surface

Fig.9 Dynamic Pressure on Absolute Flame and Relative Streamline
Left: Baseline   Right: Optimum result

In the present optimized result, the shaft-horsepower becomes small while the impeller head is maintained to be constant, and this means that the efficiency is improved. The optimized result shows that the blade height of the

optimized shape becomes smaller. This deformation means that specific speed of the impeller becomes smaller, and efficiency usually becomes worth, in the usual sense, since the flow passage becomes narrower. The surface stream lines, which are shown in Fig.8, show that large separation region occurs at the suction surface. This separation occurs in both baseline and the optimized results, but, in the optimized result, this separation region corresponds to the concave region at the suction and the hub surfaces which are shown in Fig.6. The specific speed of this impeller is quite small, therefore, to prevent a separation occurrence is difficult. By making a dent on the suction surface, the flow is forced to separate, and the separation region is "stored" in the dent. As a result, the blockage by the separation region is reduced, and the performance of the impeller seems to be improved. To clarify the above discussion, flow path and the dynamic pressure is compared between the original and the optimized shapes (Fig.9). The dynamic pressure at the separation region becomes higher than the ambient one. This is a primary cause of loss generation, and this high dynamic pressure region becomes smaller in the optimum shape. This means that the loss generation by the separation becomes smaller. As widely known, calculation of separated flow is quite difficult, but present result is an important knowledge to design a highly loaded impeller.

As mentioned above, the present results show that the optimization by genetic algorithm is effective even in such a highly loaded component. To confirm the feasibility of the multi-objective optimization, optimization on a turbine blade will be mentioned in the next section.

IV. Multi Objective Optimization on the Turbine Blade

A. Design Problem and Computational Condition

As the second step, multi objective genetic algorithm (MOGA) was applied to the turbine blade shape. The objective of this optimization is to clarify the availability of the MOGA to the highly-loaded component. The baseline blade shape is shown in Fig.10. The loading of the blade is about 10 to 20 % larger than that of the highly loaded turbine blade in the gas-turbine. This is the first stage rotor blade of the two stage turbine, and this stage is chosen since the entropy rise in the cascade is the largest. The blade is designed two dimensionally, but the blade shape is deformed three dimensionally in the optimization process. The grid number is 170 thousand and the wall Y+ is around 5.
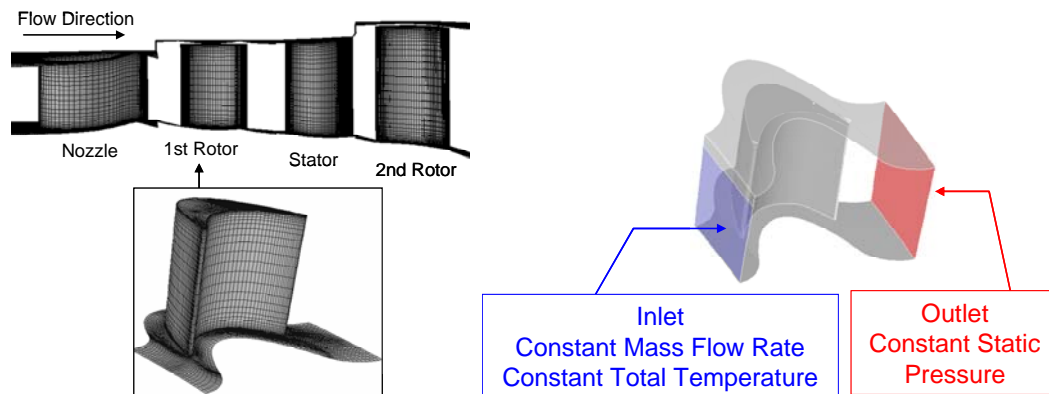

Fig.10 Baseline Blade Shape of the Turbine and the Boundary Conditions

The computational grid and boundary conditions are shown in Fig.10. Boundary conditions are important for appropriate optimization with compressible gas, since the operating point may change during the optimization process. Presently, mass flow rate, total temperature and flow angle is set to be constant, and constant static-pressure condition was applied at the outlet boundary condition.

The most important objective of the turbo-pump turbine is to generate torque to drive the pumps with lower fluid loss. In addition, the matching with the following stage is also important from a viewpoint of the total turbine performance. As a result, the following three points are selected as objective functions.

- Objective function
  - Shaft horsepower: Maximize
  - Entropy rise within the stage (Entropy Rise): Minimize
  - Angle of attack (AOA) of the next stage (Next Stage AOA): Minimize

● Constraint Function
None

Figure 11 shows the control points of the design variables. There are 8 control points in each hub, mean and tip blade section, and each control point moves to the axial and circumferential directions, except the leading and trailing edge control points at the hub. In addition to these two directional movements, scaling and rotating movements were applied to the leading and trailing edge control points. The total design variables are 58.

Blade Surface Control Points
•Radial Position
•Axial Position

Total Design Variables : 58

Leading / Trailing Edge Shape
•Curvature Radius
•Rotation
•Radial Position
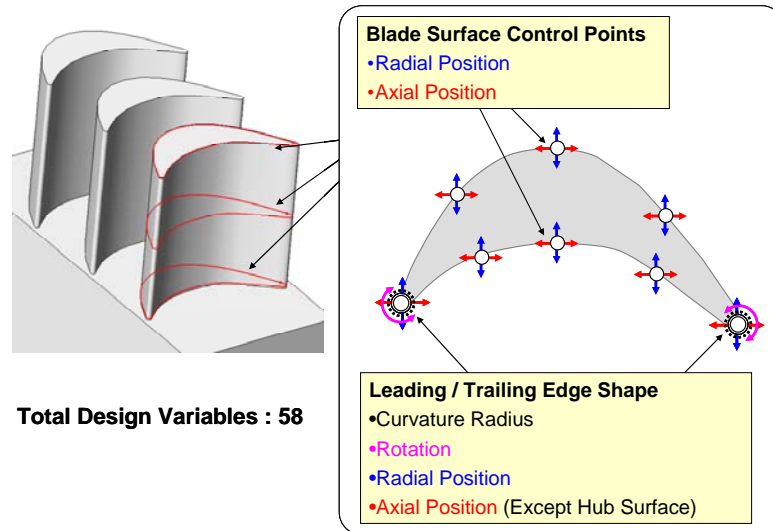•Axial Position (Except Hub Surface)

Fig.11 Control Points distribution of the Turbine

Presently, the operating condition is set to the same as the test rig condition. The rotation speed is 14000 rpm and the working fluid is air. The total generation is set to 100.

B. Optimized Results

Figure12 shows the plots of each objective functions of optimization, namely, shaft horsepower, entropy rise and next stage AOA. Each value is normalized by the baseline shape result. The maximum improvement of shaft-horsepower is about 8% increase, and entropy-rise and next stage AOA are 30% and 40% reduction, respectively. According to Fig.12, it seems that there is a strong correlation between shaft horsepower and entropy rise, and a weak correlation between next stage AOA and shaft horsepower. However, it is difficult to clarify the relation between design variables and objective functions by these two-dimensional plots. In order to know tradeoff information in multi-objective optimization, Obayashi[6] proposed to use Self-Organizing Map (SOM). The SOM projects multi-dimensional information to two-dimensional surface, and can show tradeoff information more clearly. In addition to SOM visualization, correlation function is used to reveal design tradeoff tendency. The correlation function (Corr) shows the tendency of similarity between two data arrays. If the absolute value of the correlation function is large, correlation between the selected two arrays is strong. And its sign shows tendency.
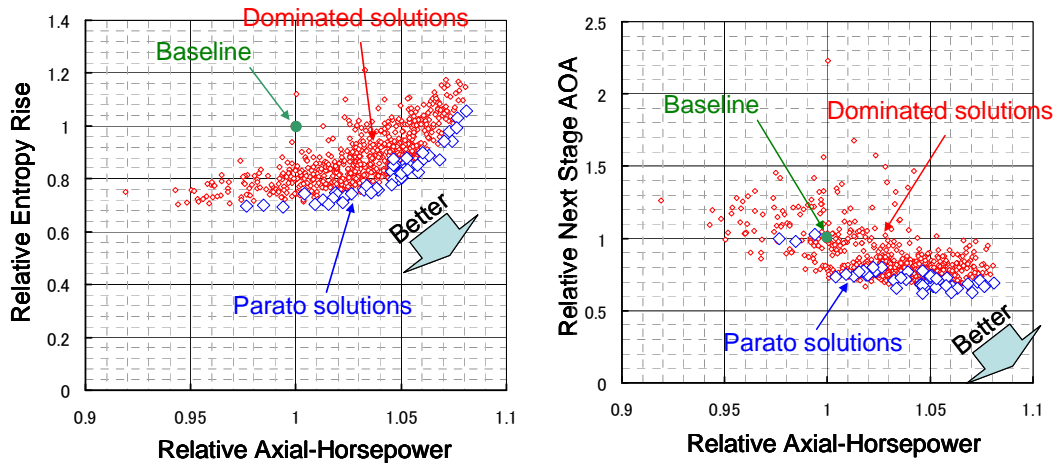
Fig.12 Plots of dominated and parato solutions

Figure 13 shows SOM and correlation functions of objective functions of the all results. According to Fig. 13, strong tradeoff can be observed between the shaft horsepower and the entropy rise, and the shaft horsepower and the next stage AOA. On the contrary, correlation between the entropy rise and the next stage AOA is weak since the correlation function between these two objective functions is small. These results shows that the turbine power output affects internal loss generation (entropy rise) and matching (next stage AOA), but the small internal loss with good matching can be achieved. According to Fig. 12, the next stage AOA does not greatly change compared to the other two objective functions. Therefore, consideration of tradeoff between shaft horsepower and entropy rise is mainly mentioned.
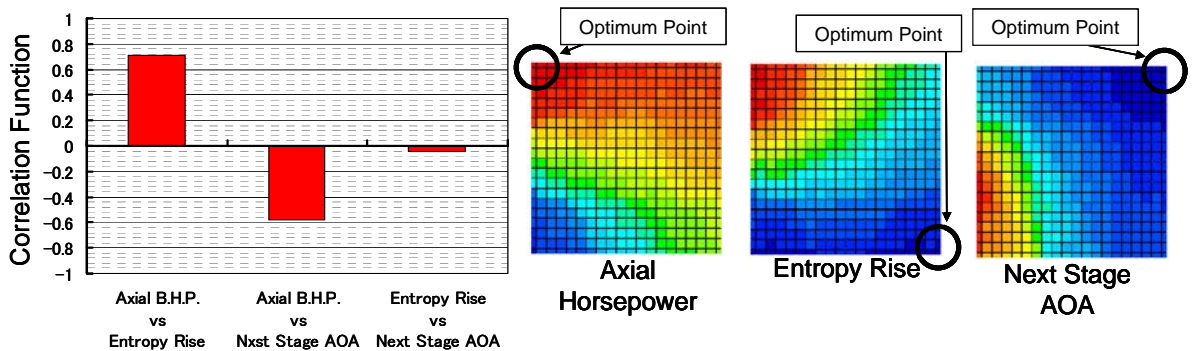

Fig.13 Correlation function (upper) and SOM (lower) of the objective functions of the all results

C. Tradeoff and Blade Shape

Figure 14 show blade shape and the pathlines of the each optimum result. It can be observed that corner separation at the blade suction side is reduced in both of the optimized results. And corner separation of the entropy-rise optimum solution becomes even smaller than that of the other two results. According to these results, the corner separation takes an important role to reduce entropy rise within the stage.

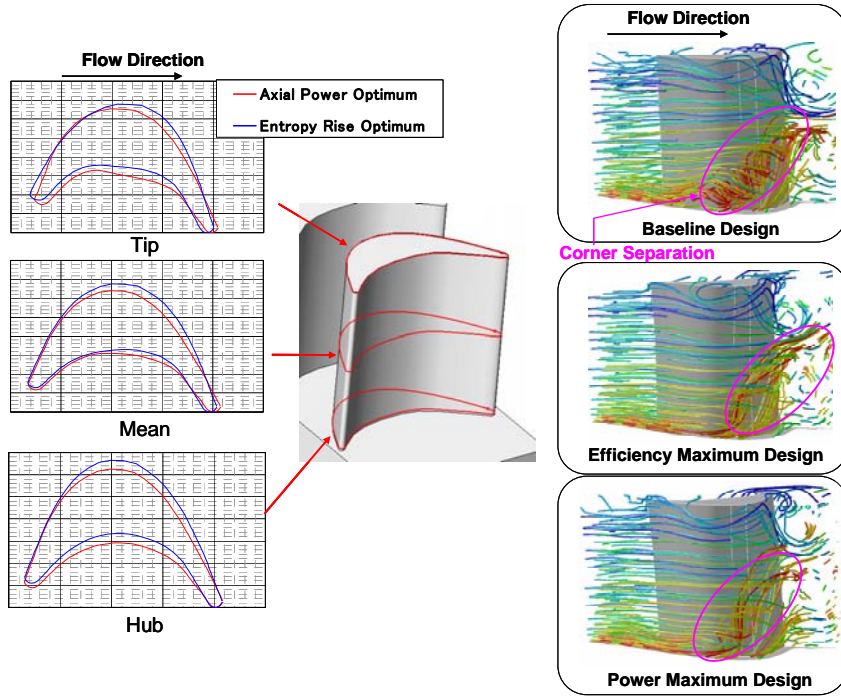American Institute of Aeronautics and Astronautics

Fig.14 Blade shape of each cross section (Left) and Pathlines colored by vorticity magnitude (Right)

From here, consideration of shaft-horsepower optimum result will be carried out. According to the ideal velocity triangle study, turbine output horsepower can be estimated as following.

$$Power = U \cdot \Delta U \cdot m_f \qquad (3)$$

In the present calculation, inlet mass flow, flow angle and rotation speed is set to be constant, therefore, tangential velocity difference is the major cause of output horsepower difference. Figure 15 shows pressure, temperature, velocity and other physical values comparison between entropy-rise optimum and shaft-horsepower optimum results. According to Fig.15, the inlet tangential velocity magnitude of shaft-horsepower optimum result becomes larger than that of entropy-rise optimum result. On the contrary, at the outlet, the tendency of the tangential velocity magnitude becomes reverse, however, the difference at the inlet is larger than that of the outlet. Therefore, it can be said that inlet velocity increase takes an important role for shaft-horsepower improvement. In order to increase the inlet velocity, the density should become lower, and Fig.15 shows that this density reduction is mainly derived from the inlet pressure reduction. One of the answers to reduce the inlet pressure is to minimize the inlet flow incidence. The control points that affects the above consideration is shown in Fig.16. The SOM in the figure shows the control points which has large correlation function to each objective functions. The trailing edge design variables also have an influence on shaft-horsepower increase, however, as described below, the trailing edge shape also affects entropy-rise within the stage.

As shown in Fig.14, reduction of corner separation takes an important role to reduce entropy rise. Figure 15 shows velocity distribution at the mid-span, and this figure clearly shows that outlet velocity becomes larger than that of shaft-horsepower maximum result. This means that, in the entropy rise optimum result, corner separation is discharged before its development by increasing the outlet velocity. This velocity increase is derived by increasing the outlet blade angle, which is shown in Fig.15, and control points that have strong correlation to entropy-rise is also sown in Fig.16.

In summary, the inlet blade angle affects shaft-horsepower improvement by increasing inlet velocity. And the outlet blade design influences both shaft-horsepower and entropy-rise by controlling corner separation.

Axial Horsepower Optimum

- -

Entropy-rise Optimum

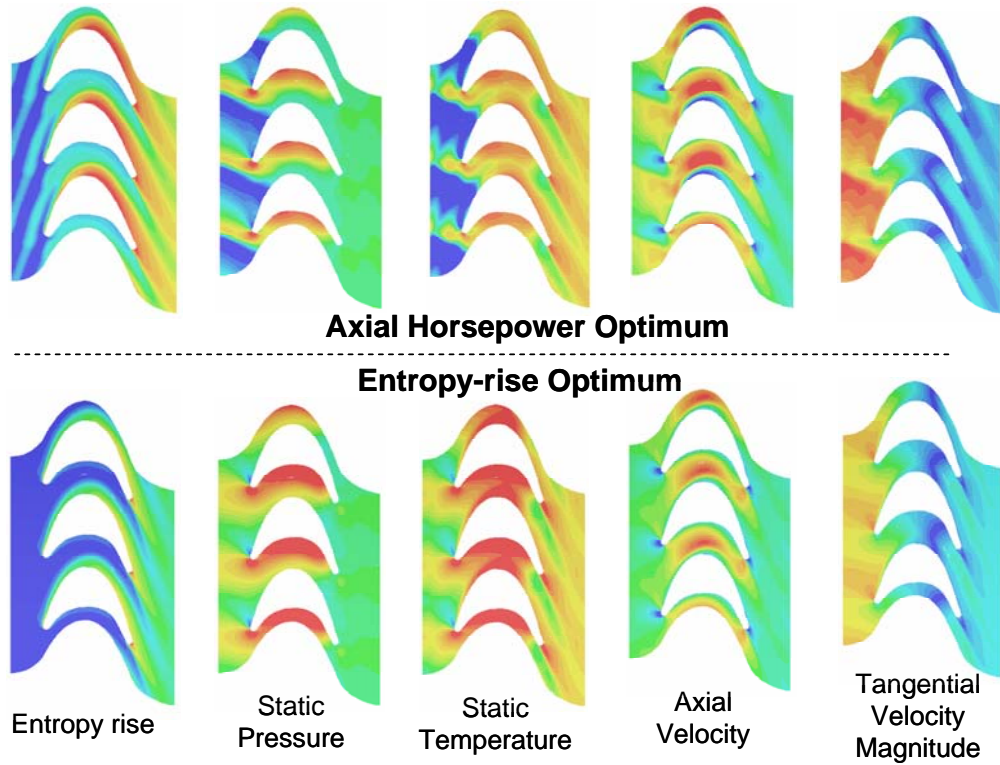| Entropy rise | Static Pressure | Static Temperature | Axial Velocity | Tangential Velocity Magnitude |

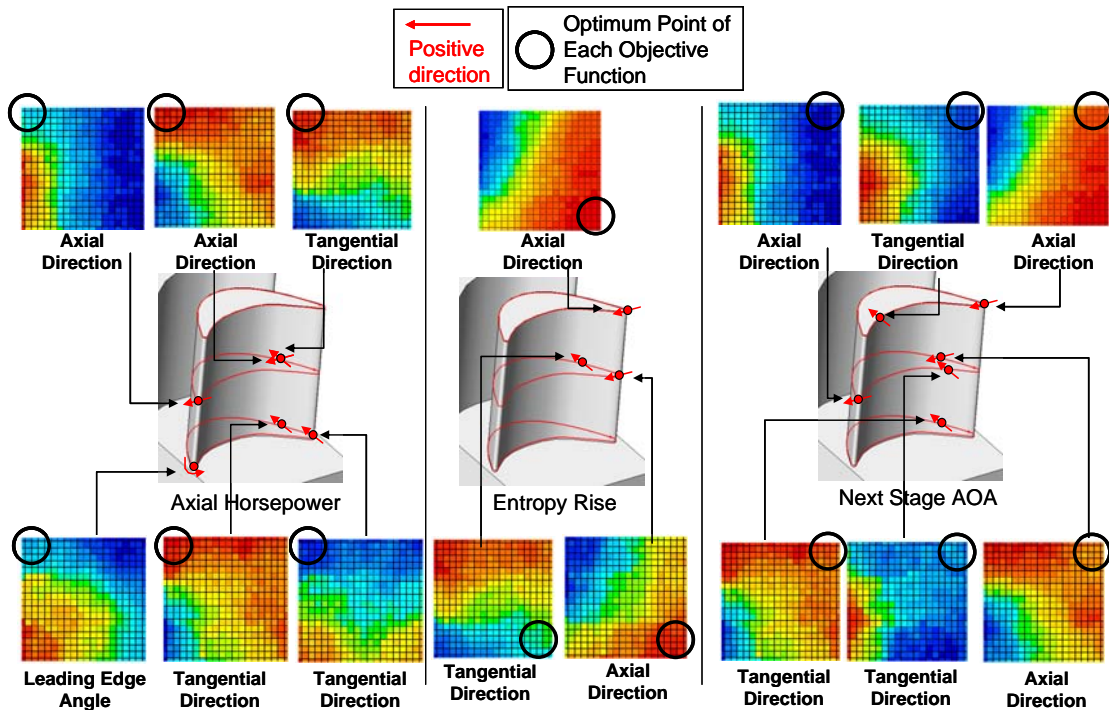Fig.15 Physical value distribution at mean section

Fig.16 Design variables and SOM which have strong correlation to each objective function

The present threshold is $\left|Corr\right| \geq 0.3$

V. Summary and Future Work

In the present study, single and multi objective optimization on blade shape design were carried out. A single objective optimization is on the impeller blade design, and a multi objective optimization is on the turbine blade design. The conclusions of the study are the followings.

- The genetic algorithm is effective in the optimization of highly-loaded impeller and turbine blades for the rocket engines.
- By use of optimization technique, performance of turbopump component is able to improve much more.
- Treatment of separation takes an important role to improve performance of both the impeller and the turbine.

Through this research, several problems are recognized. One is the high cost computational time, since hundreds of CFD calculations are required in the present optimization. To overcome this problem, genetic algorithm with Kriging interpolation [9] will be implemented near future. The other problem is the complicated preparation of the optimization. As shown in Fig.2, several different software or computational codes are used in the optimization procedure. The procedure should be processed automatically, therefore, auto running script must be written for preparation, but writing and confirming the script requires a lot of time and volume of work. To reduce such workload, integrated GUI tool is being constructed.

Acknowledgments

References

[1] Kurosu, A., et al., "Study of Next Booster Engine LE-X in Japan," *Proceedings of 42nd AIAA/ASME/SAE/ASEE Joint Propulsion Conference*, AIAA 2006-4700, Sacramento, CA, July, 2006.

[2] Negoro, N., et al., "Next Booster Engine LE-X in Japan," *Proceedings of 43nd AIAA/ASME/SAE/ASEE Joint Propulsion Conference*, AIAA 2007-5490, Cincinnati, OH, July, 2007.

[3] Oyama, A., et al., "Transonic Axial-Flow Blade Optimization Using Evolutionary Algorithms and a Three-Dimensional Navier-Stokes Solver," *AIAA Journal of Propulsion and Power*, Vol.20, No.4, 2004, pp.612-619

[4] Griffin, L.W., et al., "Design and Analysis of Turbines for Space Applications", *Proceedings of 33rd AIAA Fluid Dynamics Conference and Exhibit*, AIAA2003-3933, Orlando, FL, June, 2003.

[5] Schumacher, T., Weston, T. and Campos, F., "Automatic Optimisation of Aircraft Ventilation System Components with CFD," *Proceedings of IACC2007 on Disc [CD-ROM]*, Paris, France, 2007.

[6] Obayashi, S., Jeong, S. and Chiba, K., "Multi-Objective Design Exploration for Aerodynamic Configurations," *Proceedings of 35th AIAA Fluid Dynamics Conference and Exhibit*, AIAA2005-4666, Toronto, Ontario, June, 2005.

[7] Oyama, A, Shimoyama, K. and Fujii, K., "New Constraint-Handling Method for Multi-Objective and Multi-Constraint Evolutionary Optimization," *Transactions of the Japan Society for Aeronautical and Space Sciences*, Vol.50, Vol.157, 2007, pp.56-62

[8] Yamanishi, N., et al., "Large Eddy Simulation of Unsteady Flow in the LE-7A Liquid Hydrogen Pump," *Proceedings of 43nd AIAA/ASME/SAE/ASEE Joint Propulsion Conference*, AIAA 2007-5515, Cincinnati, OH, July, 2007.

[9] Jeong, S., Minemura, Y. and Obayashi, S., "Optimization of Combustion Chamber for Diesel Engine Using Kriging Model," *Journal of Fluid Science and Technology*, Vol.1, 2006, pp.138-146